*Marked Revision

Filtered Smith Predictor to control pH during enzymatic hydrolysis of microalgae to produce L-aminoacids concentrates

J.M. Romero-García[a,*], J.L. Guzmán[b], J.C. Moreno[b], F.G. Acién[a] and J.M. Fernández[a]

[a] *Department of Chemical Engineering, University of Almería, 04120, Almería, Spain.*

[b] *Department of Computer Science, University of Almería, 04120, Almería, Spain.*

E-mail addresses: juanmiguelrg@ual.es (J.M. Romero-García), joguzman@ual.es (J.L. Guzmán), jcmoreno@ual.es (J.C. Moreno), facien@ual.es (F.G. Acién), jfernand@ual.es (J.M. Fernández).

Author for correspondence:

J.M. Romero-García

Department of Chemical Engineering, University of Almería

La Cañada de San Urbano, Almería 04120, Spain

Telephone: +34 950 015484; fax: +34 950 015484; e-mail: juanmiguelrg@ual.es

Abstract

The main step of the production of L-aminoacids concentrates from microalgae is the enzymatic hydrolysis. This process has to be done at the optimum temperature and pH of the enzyme in order to obtain the maximum yield. In order to keep a constant pH, NaOH (1M) or H_2SO_4 (1M) are used, depending on the reaction step. When working with pH it is not possible to use the governing equations due to the complexity of the enzymatic hydrolysis. In this work, the modelling of pH is experimentally performed on a laboratory scale plant. Since the obtained model presents delay and uncertainty in the parameters, a Filtered Smith Predictor is proposed as control strategy. This control scheme has been tested in the real system. The Filtered Smith Predictor has reduced the Integral Absolute Error and the time for the solution addition in more than 25% and it has increased 5% the production of L-aminoacids compared to an on-off control, which is the controller most used in these processes.

Keywords: batch bioprocess**,** enzymatic hydrolysis, microalgae free-aminoacids, nonlinear dynamics, pH robust control, Filtered Smith Predictor.

1. Introduction

Currently, the abatement and valorisation of CO_2 pose an extraordinary challenge that must be tackled with different technologies. One possibility is a biological treatment with photosynthetic microorganisms to generate biomass that could be then converted into products with energetic or industrial interest. Nowadays, there is great interest on biofuel production from photosynthetic microorganisms, such as microalgae and cyanobacteria.

Technology is being developed and scaled-up to demonstrate the viability of the process. The oil content of microalgae biomass is most commonly between 10 and 30%, but this upper limit is only

Abbreviations: AU, Anson Units; BSA, Bovine Serine Albumin; DTC, Dead-Time Compensator; EEFC, Estación Experimental Fundación Cajamar; FBG, Fungal Beta Glucanase; FSP, Filtered Smith Predictor; IAE, Integral Absolute Error; LAPU, Leucine Amino Peptidase Units; OPA, Ortofenilaldehide; PI, Proportional Integral; PWM, Pulse-Width Modulation; SCADA, Supervisory Control And Data Acquisition; SP, Smith Predictor.

obtained under stressing conditions. Besides lipids, other major components in the microalgal biomass are carbohydrates (20-30%), ash (5-10%) and proteins (30-60%) (Rebolloso et al., 2000, 2001). For high growth rate cultures, which are usually the most productive in term of biomass, proteins are the most abundant component in the biomass, representing more than 45% of the total dry weight (Acién et al., 1998, 2000). Therefore, the production of large amounts of lipids from microalgae involves the production of a large deal of protein. So, it is clear that the protein produced must be valorised to make the process economically positive. Proteins from microalgae can be used for human and animal nutrition (Spolaore et al., 2006), but in both cases enzymatic hydrolysis is recommended to improve the digestibility of cell proteins as most microalgae are indigestible to monogastric animals and humans (Morris, 2008). Microalgae biomass has also been proposed as biofertilizer by its aminoacid profile and its content in other algae-derived natural substances (Ördög et al., 2004). It has been demonstrated that the application of aminoacids in foliar (Jie et al., 2008) and soils (Mitchell et al., 1994) has a favourable effect on plants. By-products from meat and from vegetal origin (pea meal, soya flour, sunflower) have been successfully tested to obtain them (Kubo et al., 1994; Ordóñez et al., 2001; Soetrisno and Holmes, 1992; Tejada and González, 2003).

Recently, a process for the production of free-aminoacids concentrates from microalgal biomass of *Scenedesmus almeriensis* is developed (Romero-García et al., 2012). The method is based on the enzymatic hydrolysis of proteins contained in the biomass. The enzymatic reaction step has been optimized in addition to the pre-treatment step necessary to improve the yield of the process. During the enzymatic hydrolysis, optimal conditions of pH and temperature of the enzymes must be maintained, in order to achieve the greatest degree of hydrolysis. The temperature control problem is relatively straightforward since the dynamic equations that define the heat transfer are well-known (Bouhenchir et al., 2006; Hua et al., 2004; Macků and Sámek, 2010). However, in the case of pH, the dynamics is often quite complicated to be modelled and controlled. The main reason is

due to: (i) the complexity of the substrate used, since this is a new source of protein, and (ii) the enormous complexity of the enzymatic hydrolysis of proteins (in this case, free-aminoacids are produced, which cause the variation of pH). This fact is due to a single reaction, but rather a set of simultaneous reactions of bond breaking with different reactivity and different charged species in equilibrium, products that are further substrates for the process, inhibition and inactivation of the enzyme, etc. (Guadix et al., 2000; Margot et al., 1997); neutralization equations between acid and basic species that participate in the process are unknown.

In this work, an experimental simplified model has been obtained for control purposes. The main features of the resulting dynamics are that the process presents dead time and that the process model parameters are time varying with respect to the current operating point (Carrasco et al., 2009; Sing and Postlethwaite, 1997; Wright and Kravaris, 1991). The main reason of this resulting dynamics is that significant pH deviations are obtained due to the H^+ released from the hydrolysis reaction. This fact can be compensated by adding base, but an adequate control strategy is required to avoid providing base in excess. Conventional strategies for the control of pH (PI, on-off) are still the most used in industry for these processes, because of its simplicity and ease of implementation, but their lack of ability to handle nonlinear processes, long time delays or large uncertainties, reduces the efficiency of the control, hindering the process (Gaberalla et al., 2008; Palancar et al., 1996; Williams et al., 1990). In particular, the presence of a delay in the control loop can have negative effects on the control system performance. For instance, the presence of significant dead time can result in oscillatory responses or long delays in the disturbance rejection (Normey-Rico and Camacho, 2007). Furthermore, when the process dynamics is time varying or when there is uncertainty in the process parameters, the control loop must be designed to face these situations since otherwise the control system can lead to a poor performance or instability. Such as commented above, in the case studied in this work, the enzymatic hydrolysis of protein, both

features dead time and changing dynamics are observed and thus an adequate control strategy is required to obtain a desirable performance.

Improving the process control can therefore be expected to increase the yield of the process and to save reactants, which also prevents the accumulation in the hydrolizate of salts resulting from the neutralization of excess acid and base added by an inadequate control. Laboratory experiences carried out to model the pH in this specific process have shown that the dynamic parameters for pH contain uncertainty, in such a degree as to request a robust control strategy, as well as significant dead time. In view of this, a Filtered Smith Predictor (FSP) has been selected as control strategy, capable of taking into account the delay (as a classical Smith Predictor (SP) control scheme) and assuring the robustness (Normey-Rico and Camacho, 1999, 2007, 2009; Roca et al., 2009, 2011; Santos et al., 2010).

2. Materials and methods

2.1. Microalgae biomass

The raw material used for the experiments was dry-freezed biomass of the freshwater strain *Scenedesmus almeriensis*. The biomass was produced in continuous mode at 0.3 1/day in an industrial size tubular photobioreactor (3 m^3) at Estación Experimental Fundación Cajamar (EEFC) located in Almería, Spain (see Fig. 1). The biochemical composition of the biomass was: 41.8% proteins, 11.2% lipids (8.5% fatty acids), 38.7% carbohydrates, and 8.3% ash.

2.2. Enzymes

In the hydrolysis process, three liquid commercial enzymatic complexes were used, supplied by Novozymes A / S (Bagsvaerd, Denmark), which have the following characteristics:

- Alcalase 2.5L: is obtained by submerged fermentation of a strain of *Bacillus licheniformis* whose main component is subtilisin A (Carlsberg subtilin) endoprotease activity, standardized by the manufacturer to 2.5 AU/g, standardized by the modified process Anson.
- Flavourzyme 1000L: a fungal enzyme complex, obtained by fermentation of a selected variety of *Aspergillus oryzae* that has not been genetically modified, and contains both endoprotease activity and exoprotease, standardized by the manufacturer in 1000 LAPU/g.
- Viscozyme L: a fungal multienzyme complex, containing carbohydrases including arabinase, cellulase, β-glucanase, hemicellulase and xylanase, obtained by fermentation of a selected variety of *Aspergillus aculeatus*, and β-glucanase activity, standardized by the manufacturer in 100 FBG/g.

2.3. Chemicals

The chemicals used for analytical methods were sodium tetraborate decahydrate, DL-Dithiothreitol, Phthaldialdehyde, Dodecyl sulphate and DL-Serine from SIGMA-ALDRICH. Furthermore, ethanol, Bovine Serine Albumin, Copper (II) sulfate-pentahydrate, Dodecylhydrogensulphate Sodium Salt, Folin-Ciocalteu´s phenol reagent, Potassium Sodium Tartrate tetra hydrate, Sodium carbonate, Sodium hydroxide and Sulfuric acid from Panreac were used.

2.4. Protein content and hydrolysis degree

The protein content of samples was determined using a modification of the Lowry method (González et al., 2010), with BSA as standard. The hydrolysis degree was measured using the OPA method with serine as standard (Nielsen et al., 2001). This method is based on the reaction of ortofenilaldehide (o-phthaldialdehyde) with free α-amine groups giving a derivative that can then be measured spectrophotometrically at 340 nm to quantify the amount of free α-amine groups in the

sample. According to this method, the following values of the parameters of the model have been selected α=1, β=0.4, and h_{tot}=8.

2.5. Production of L-aminoacids concentrates by enzymatic hydrolysis

The process proposed in (Romero-García et al., 2012) is summarized in the block diagram shown in the Fig. 2. According to the proposed process, the cells must be disrupted mechanically, by milling (horizontal-bed ball-mill, 20 cm radius at 40 rpm), previously to be processed. Next, the biomass, at maximum biomass concentrations of 270 g/l, is treated with Viscozyme L for 30 min at 50ºC and pH=7 to reduce its viscosity. Then the enzymatic hydrolysis is performed (twice for 3 hours period), in which biomass proteins are transformed into free amino acids by the action of enzymes on peptide bonds, which break it releasing the amino group and carboxyl group which may be partially ionized, depending on the pH of the medium. The enzymes must work in optimal conditions of temperature and pH. This stage has a combined action of two enzymes. The first one is the Alcalase 2.5L (endoprotease), that breaks peptide bonds within the protein chains, and its optimal working conditions are 50 °C, a pH of 8 and a time action of 2 hours (Kechaou et al., 2009; Ovissipour et al., 2009; Tang et al., 2009) (adjusted with NaOH 1M). Afterwards, Flavourzyme 1000L (exoprotease) is added, that breaks peptide bonds outside, and its optimal working conditions are 50 °C, pH 7 and reaction time of 1 hour (Kechaou et al., 2009; Tang et al., 2009) (adjusted with H_2SO_4 1M).

During hydrolysis of the peptide bond (Eq. (1)) at alkaline pH between 7 and 10, the carboxyl group is fully dissociated (Eq. (2)) and the amino group is partially protonated (Eq. (3)). Therefore, for every mole of hydrolyzed peptide bonds there is a monovalent anion mol, P-COO^-, one mole of monovalent cations H^+ and one shared between the two species P-NH_3^+ and H^+, which lead to a continuous lowering of pH (Guadix et al., 2000). Therefore, it is necessary to control the pH in order to make the enzymes work in their optimum pH ranges. For that reason, an alkali is added to

neutralize these protons and thus achieving the stability of the pH. The protons are replaced by the cation of the base, thus the moles of added alkali (NaOH) are equivalent to the protons generated by hydrolysis, which is only a fraction of hydrolyzed amino bonds.

$$P\text{-}CO\text{-}NH\text{-}P + H_2O \rightarrow P\text{-}COOH + P\text{-}NH_2 \quad (1)$$

$$P\text{-}COOH \rightleftharpoons P\text{-}COO^- + H^+ \quad (2)$$

$$P\text{-}NH_3^+ \rightleftharpoons P\text{-}NH_2 + H^+ \quad (3)$$

Once the reaction has been performed, the enzymes can be deactivated and precipitated by heating at 75ºC for 15 minutes. The supernatant containing the free-aminoacids concentrate can be finally separated from the waste biomass, with low nitrogen content, by centrifugation.

2.6. Experimental equipment

Fig. 3 shows the schematic diagram of the laboratory scale equipment. This system is composed of a thermostat bath to maintain the optimum working temperature of the enzymes (50 °C), which includes an electrical resistance with stirrer to homogenize the temperature of the water (Microterm 520 W, JP Selecta SA) and a temperature sensor (PT-100). A glass BSTR (Batch Stirred-Tank Reactor) of 9 cm diameter and 18 cm height, equipped with a 3 cm diameter Rushton turbine, temperature and pH sensors (PT-100; probe: InPro3030, Mettler-Toledo, Transmitter: pH Transmitter 220-R1, CRISON). A pulse pump (Class 5 On-Off, 5-5 l/h-bar, CTX), which will be responsible for providing the flow of NaOH (1 M) and H_2SO_4 (1M) for pH adjustment, is also installed. The pump provides flow rates higher than required, so the flow is byapassed to its output in order to achieve the desired value. All sensors, pump and electrical resistance are connected to an input-output card (LabJack U12, LabJack Corporation), which is connected via USB to the control computer, which also performs the function of data storage. Fig. 4 shows the schematic diagram of industrial control of enzymatic hydrolysis.

2.7. Experimental operation mode

First, the temperature is adjusted to 50 ºC and pH to 7 for adding Viscozyme L, which reacts for 30 min. Afterwards, the pH is adjusted to 8 and Alcalase 2.5L is added. At this time, the enzymatic hydrolysis starts. During the two hours that this enzyme acts, step changes with constant flow rate of NaOH (1M) are made in order to produce variations of pH near to 8, which is then used to model pH in the first part of the hydrolysis process. Finally, the pH is adjusted to 7 for adding Flavourzyme 1000L, which reacts during two hours more. At this time, step changes with constant flow rate of H2SO4 (1M) are introduced to produce variations of pH near to 7, which is then used to model the pH in the second part of the hydrolysis process.

2.8. Reaction curve method

The reaction curve method is used to adjust the previous experimental results on the pH behaviour to a linear time invariant model. The method consists in applying a step change at the input of the open-loop system to capture the process dynamics (Fig. 5). From the resulting response, the process parameters can be obtained (if possible) as a first-order model with dead time such as described by Eq. (4),

$$\frac{Y(s)}{U(s)} = \frac{K}{\tau \cdot s + 1} \cdot e^{-L \cdot s} \tag{4}$$

where K is the *static gain*, which is the quotient between the change in the output amplitude in steady state and the input step amplitude (see Eq. (5)), L is the *delay time*, or time lapse during which the output of the system does not react after the step is produced in the input (see Eq. (6)), and τ is the *time constant*, that is the time elapsed since the instant in which the output starts to evolve after the delay to that in which it reaches the 63% of its new steady state value (see Eq. (7)). The method was proposed by Cohen and Coon (1953) and it is based on drawing a tangent to the curve at the point of maximum slope, and from this the parameters are defined by the following equations (Fig. 5):

$$K = \frac{\Delta y}{\Delta u} \tag{5}$$

$$L = t_L - t_0 \tag{6}$$

$$\tau = t_{63} - L \tag{7}$$

2.9. Smith Predictor (SP)

It is the first control system proposed in the literature that includes a delay compensator, and it is probably the most well-known and used in practice to solve the control of systems with delay, being proposed by Smith (1957) for monovariable systems. This system is known as the Smith Predictor (SP) or dead-time compensator (DTC). Fig. 6 shows the structure of the SP. The blocks *C(s)* and $P(s)$ correspond to the controller and the real plant respectively, with $P(s) = G(s) \cdot e^{-Ls}$, where L is the delay. This structure feeds back the predicted output of the process, calculated using a model of the plant without delay $G_n(s)$. Furthermore, to offset the effect of disturbances and correct the effects of modelling errors, it also feeds back the difference between process output and model output including the estimated delay ($P_n(s) = G_n(s)\, e^{-L_n s}$).

However, the SP has been the subject of many investigations that have produced as main results the detection of some constraints on the behavior of the system. The most important ones are: to be sensitive to small modelling errors that can make the closed loop systems unstable; its single degree of freedom structure cannot be used for open-loop unstable processes; and cannot reject constant disturbances in steady state when the plant is an integrator (Normey-Rico and Camacho, 2007).

The next section briefly describes one of the proposed solution to these problems (Martínez and Camacho, 2005), which is the one used in this work.

2.10. Filtered Smith Predictor (FSP)

Among the DTCs proposals, FSP proposed by Normey-Rico and Camacho (2009) is selected, which has two main characteristics highly valued in the practical environment: simplicity and robustness features.

The structure proposed by Normey-Rico and Camacho is shown in Fig. 7. As can be seen, corresponds to the basic structure of the Smith Predictor shown in Fig. 6, but adding a filter ($F_r(s)$) to enhance robustness. Note that if $F_r(s)$ is a low-pass filter, then the robustness of the system is improved. Moreover, if there are not disturbances ($q(t) = 0$) the closed-loop system in its nominal form is not affected by the inclusion of $F_r(s)$.

The design of $C(s)$ and $F_r(s)$ is done to achieve the performance and the required robustness, which are given by Eqs. (8) and (9) respectively.

$$H_q(s) = P_n(s) \cdot \left[1 - \frac{C(s) \cdot P_n(s) \cdot F_r(s)}{1 + C(s) \cdot G_n(s)} \right] \tag{8}$$

$$dP(\omega) = \frac{\left|1 + C(j\omega) \cdot G_n(j\omega)\right|}{\left|C(j\omega) \cdot P_n(j\omega) \cdot F_r(j\omega)\right|} \tag{9}$$

To consider the effect of modelling errors (Fig. 8), it is assumed that the uncertainties can be described by an unstructured model (see Eq. (10)) (Normey-Rico and Camacho, 2007).

$$P(s) = P_n(s) \cdot \left(1 + \delta P(s)\right) = P_n(s) + \Delta P(s) \tag{10}$$

Under this hypothesis, the robust stability condition for the FSP is as shown in Eq. (11), where $\overline{\delta P}(\omega)$ is the uncertainty in multiplicative form given by Eq. (12), which, from Eq. (9), can be rewritten as shown in Eq. (13). Representing the terms as shown in Eq. (13), it is possible to check whether the designed filter satisfies the robust stability condition.

$$\overline{\delta P}(\omega) < dP(\omega) \;\; \forall \omega > 0 \tag{11}$$

$$\delta P(\omega) = \frac{\Delta P(\omega)}{P_n(j\omega)}, \overline{\delta P}(\omega) = \frac{\overline{\Delta P}(\omega)}{\left|P_n(j\omega)\right|} \quad \forall \omega > 0 \tag{12}$$

$$\frac{\left|1+C(j\omega)\cdot G_n(j\omega)\right|}{\overline{\delta P}(\omega)\cdot\left|C(j\omega)\cdot P_n(j\omega)\right|} > \left|F_r(j\omega)\right| \quad \forall\omega>0 \tag{13}$$

3. Results and Discussion

3.1. pH modelling

Modelling of the pH during the hydrolysis cannot be performed by a set of differential equations relating the change in pH and the NaOH (1M) (Q_l) or H_2SO_4 (1M) (Q_s) flows along the hydrolysis reaction since as described above. Therefore, an experimental modelling is performed to obtain the dynamic model of the system by the reaction curve method described in section 2.8. Three open-loop experiments were carried out for calibration purposes, and other three for the validation procedure, in which the flow of solution of NaOH (1M) (Q_l) and H_2SO_4 (1M) (Q_s) was varied. In all experiments there is a pH change of 8-7 (pulse with red vertical line in Fig. 9-11), to change the first part to the second part of the hydrolysis process (see section 2.7). In the following, the three experiments used for calibration are described.

Experiment 1: four pulses are given in the first 2 hours of reaction with NaOH (1M), 5 min each pulse, at a rate of 1.12 ml/min. In the next 2 hours, two pulses with H_2SO_4 (1M) are given, 2 min each one, at a flow rate of 0.69 ml/min, but both have been discarded for problems with agitation (Fig. 9).

Experiment 2: in this experiment, there are five pulses with NaOH (1M), 5 min each one, at a flow rate of 0.74 ml/min in the first 2 hours of reaction. In the next 2 hours, there are two pulses with H_2SO_4 (1M), 2 min each one, at a flow rate of 0.52 ml/min (Fig. 10).

Experiment 3: three pulses are given in the first 2 hours of experiment with NaOH (1M), 5 min each one, with a flow of 1.37 ml/min. In the next 2 hours, there are two pulses with H_2SO_4 (1M) for 2 min each one, having a flow of 1.57 ml/min (Fig. 11).

From these results, the process dynamics was analyzed and captured for each individual pulse following the next two steps:

1. First, and due to the noisy result obtained in the pH signal, a filter was used to reduce that noise, allowing a much more accurate modelling procedure. The pH signal is passed through a filter as shown in Eq. (14). For this filter, the value of τ_f was set to 5 seconds in order to mitigate the noise and to avoid information losses.

$$Filter \Rightarrow \frac{1}{\tau_f \cdot s + 1} \tag{14}$$

2. Then, according to the dynamics observed from the open-loop experiments, the system can be modeled by a first-order process with delay (Eq. (15)). Thus, the reaction curve method can be used to calculate the process model from the experiments such as described above.

$$\frac{pH(s)}{Q(s)} = \frac{K}{\tau \cdot s + 1} \cdot e^{-L \cdot s} \tag{15}$$

The results obtained for the static gains (K), time constants (τ) and dead times (L) are shown in Table 1.

The resulting models were simulated in Simulink® (MathWorks, Inc.) and their responses were validated using the other three experiments. Fig. 12 shows two examples of the validation results for pulses 2 and 6. For all pulses, a first-order model with delay and uncertainty in model parameters is obtained. The resulting models for the two parts in the process are as follows:

$$\frac{pH(s)}{Q_l(s)} = \frac{[0.16,0.43]}{[200,226] \cdot s + 1} \cdot e^{-[43,92] \cdot s} \tag{16}$$

$$\frac{pH(s)}{Q_s(s)} = \frac{[-0.33,-0.27]}{[55,62] \cdot s + 1} \cdot e^{-[16,19] \cdot s} \tag{17}$$

where now the model parameters are within a range, indicating the uncertainty of the process. Notice that the process is really described by a time-varying dynamics, but in this work, this changing dynamics has been handled as uncertainty. High-order models could have been used to

capture the process dynamics in a more precise way and thus reducing the model uncertainties. However, these high-order models would have to be approximated by low-order models in order to use them for control purposes. Thus, in this work low-order models are directly proposed.

3.2. pH control

The design of $C(s)$ and $F_r(s)$ of the FSP is performed according to the method proposed in Normey-Rico and Camacho (2009) for stable plants with dead time. This method is used as follows:

- Calculate $C(s)$ as a PI controller (Eq. (18)) from the nominal model (Eq. (19)), where the nominal model describes a representative model for the resulting uncertain models Eqs. (16) and (17) (the mean value for the static gain (K_n), time constants (τ_n) and dead times (L_n) is used as nominal). Then, $\tau_I = \tau_n$ and $K_p = \tau_n / (\tau_r \cdot K_n)$, where τ_r defines the closed-loop poles (poles assignment), are chosen.

$$C(s) = K_p \cdot \left(1 + \frac{1}{\tau_I s}\right) \tag{18}$$

$$P_n(s) = \frac{K_n}{\tau_n \cdot s + 1} \cdot e^{-L_n \cdot s} \tag{19}$$

- Calculate $F_r(s)$ from the algorithm in Normey-Rico and Camacho (2009), where $F_r(s)$ can be calculated as shown in equation (22), where $D_{cl}(s)$ is the polynomial whose roots are the poles of the closed-loop system, $N_c(s)$ is the numerator of controller function and $N_n^-(s)$ is a polynomial of the numerator of nominal model whose roots are in the left half plane.

$$N_o(s) = 1 + \tau_n \cdot \left[1 - \left(1 - \frac{\tau_o}{\tau_n}\right)^2 \cdot e^{-L_n/\tau_n}\right] \cdot s \tag{20}$$

$$D_o(s) = (1 + \tau_o \cdot s)^2 \tag{21}$$

$$F_r(s) = \frac{N_r(s)}{D_r(s)} = \frac{D_{cl}(s)}{N_c(s) \cdot N_n^-(s)} \cdot \frac{N_o(s)}{D_o(s)} \tag{22}$$

- Finally, and considering the process uncertainty, parameter τ_o in Eq. (21) is tuned in order to obtain the best balance between robustness and performance, according to Eqs. (11)-(13).

Hence, the previous design method has been applied to the problem presented in this paper and thus using the model data described in Table 1. First, the nominal models for uncertain models in Eqs. (16) and (17) are selected (using the mean value of the uncertainty range for each parameter), as shown below:

$$P_{n\,NaOH(1M)}(s) = \frac{0.29}{213 \cdot s + 1} \cdot e^{-70 \cdot s} \tag{23}$$

$$P_{n\,H_2SO_4(1M)}(s) = \frac{-0.3}{59 \cdot s + 1} \cdot e^{-18 \cdot s} \tag{24}$$

So, the previous procedure must be performed for each case, with solution of NaOH (1M) and H_2SO_4 (1M), respectively. For NaOH (1M), a $\tau_r = 180$ seconds is used, and for H_2SO_4 (1M) a $\tau_r = 50$ seconds is set. This makes the response of the closed-loop system 15% faster than the open-loop nominal case. Therefore, the PI controllers obtained are shown in Eqs. (25) and (26).

$$C_{NaOH(1M)}(s) = 4.08 \cdot \left(1 + \frac{1}{213 \cdot s}\right) \tag{25}$$

$$C_{H_2SO_4(1M)}(s) = -2.82 \cdot \left(1 + \frac{1}{59 \cdot s}\right) \tag{26}$$

Then, $F_r(s)$ must be set taking into account the process uncertainty and tuning τ_o until reaching a compromise between performance and robustness. The results for the selected filters are shown in Fig. 13 and Fig. 14, where both filters are designed, satisfying the robust stability condition described by equation (13), which is shown in green in the figures.

The resulting filters are obtained as shown in Eqs. (27) and (28), being $\tau_o = 140$ seconds for action with NaOH (1M) and $\tau_o = 40$ seconds with H_2SO_4 (1M), and adding a real pole at the frequency of 1 rad/s in order to contribute to the noise reduction.

$$Fr_{NaOH(1M)}(s) = \frac{35067 \cdot s^2 + 374.82 \cdot s + 1}{19600 \cdot s^3 + 19880 \cdot s^2 + 281 \cdot s + 1} \quad (27)$$

$$Fr_{H_2SO_4(1M)}(s) = \frac{2745.5 \cdot s^2 + 104.49 \cdot s + 1}{1600 \cdot s^3 + 1680 \cdot s^2 + 81 \cdot s + 1} \quad (28)$$

After obtaining the controllers and filters transfer functions, all of them are discretized with a sampling time of 10 seconds in the case of NaOH (1M) and 3 seconds in the case of H_2SO_4 (1M) ($\approx \tau_n/20$). Afterwards, the resulting control law is simulated in order to test if the system behaves correctly against the uncertainty of the models. The results are shown in Fig. 15 for a set point of pH=8 for NaOH (1M) and a pH of 7 for H_2SO_4 (1M). It is possible to observe how the responses are stable reaching the reference and providing acceptable performance results despite of the changes in the parameters.

Then, in order to show the advantages of the proposed control scheme, a comparative analysis is presented for the uncertainty in the delay, and comparing the FSP with the original SP scheme (without the filter $F_r(s)$), and with a PI controller robustly designed for stable plants with $\tau/L \geq 2$, according to the rules in Eqs. (29)-(31) from Normey-Rico and Camacho (2007). The robust PI and SP were designed using the nominal model for both part of the hydrolysis process (see Eqs. (23) and (24)).

$$P(s) = \frac{K \cdot e^{-L \cdot s}}{\tau \cdot s + 1} \cong \frac{K \cdot e^{-L \cdot s}}{\tau \cdot s} = \frac{K_v}{s} \cdot e^{-L \cdot s} \quad (29)$$

$$C_{PIrobust}(s) = K_p \cdot \left(1 + \frac{1}{\tau_I s}\right) \quad (30)$$

$$K_p = \frac{0.9}{K_v \cdot L} \quad ; \quad \tau_I = 3.37 \cdot L \quad (31)$$

The results are shown in Fig. 16 and Fig. 17, which show that the FSP has a faster response than the SP and the robust PI, being the robust PI controller that with poorest performance. The modelling error in the delay used for these results were L=90 seconds for the first part of the

process of hydrolysis and the second part L=19 seconds, which are the biggest dead time found in the modelling step.

Finally, as the actuator has saturation (the control signal is limited), the control scheme is completed with an anti-windup method, as shown in Fig. 18. This anti-windup control is described by Eqs. (32) and (33), whose discretization, approximating the integrals to successive additions, is shown in Eqs. (34) and (35).

$$v(t) = K_p \cdot \left[e(t) + \frac{1}{\tau_I} \cdot \int e(t) dt \right] + \frac{1}{\tau_I} \cdot \int e_a(t) dt \tag{32}$$

$$e_a(t) = u(t) - v(t) \tag{33}$$

$$v(z) = p_{00} \cdot [q_0 \cdot e(z) + q_1 \cdot e(z-1)] + p_{00} \cdot v(z-1) + p_{00} \cdot p_0 \cdot u(z-1) \tag{34}$$

$$q_0 = K_p \cdot \left[1 + \frac{T}{\tau_I} \right]; \;\; q_1 = -K_p; \;\; p_0 = \frac{T}{\tau_I}; \;\; p_{00} = \frac{1}{1 + p_0} \;\; (T = \textit{sample time}) \tag{35}$$

Once the control system is verified in simulation, the control structure is implemented in the experimental system, which includes a PWM to simulate a continuous change in the flow of the pump, since its flow is fixed (1.2 ml/min). The real experiments can be seen in Fig. 19 and Fig. 20, comparing these with an on-off control (Reference ± 0.05), which is a typical control for these processes. In both figures it can see the presence of noise in the signal, to which the proposed control scheme has an adequate behavior (Santos et al., 2010). Fig. 19 shows that the rise time of the FSP + anti-windup is approximately equal to the on-off, which means that it is very fast. The IAE and the injection time of the pump are calculated for both process stages and for the two control schemes (on-off and FSP) used in the real system. The FSP + anti-windup, for both stages, has reduced IAE in more than a 26% respect on-off, leading to an increased production of aminoacids nearly 5%, passing the hydrolysis degree of 51% to 53.5% because the enzymes are more time on its optimum working pH. The data here reported showed hydrolysis degrees up to

53% when both enzymes were combined as described. Morris et al. (2008) report substantially lower yields when working with *Chlorella vulgaris*, obtained a maximum hydrolysis degree of 20%, even with a previous extraction of the protein fraction using ethanol, which dropped to a 10% yield if the hydrolysis was done without previous extraction. This low yield of enzymatic hydrolysis working with *Chlorella vulgaris* could be due to their thick cell wall or to a poor choice of adequate enzymes. The highest free-aminoacids concentration achieved in a single enzymatic hydrolysis step was 49 g/l. Using *Chlorella vulgaris*, a maximum free-aminoacids concentration of 39 g/l were obtained, decreasing substantially when processing biomass concentrations over 200 g/l (Morris et al., 2008). The injection time is also reduced in more than a 25%, which will produce savings in energy and solutions (NaOH (1M) and H_2SO_4 (1M)). All results are shown in Table 2.

4. Conclusions

Modelling of the pH from experimental data using the reaction curve has led to a first-order model with delay for both reaction steps (addition of NaOH (1M) or H_2SO_4 (1M)), where the nonlinear behaviour of the system has been modelled as uncertainty in the parameters. It has been shown that the election and design of the FSP + anti-windup, in both hydrolysis steps with both enzymes, has been satisfactory since it has achieved an acceptable performance despite the uncertainty of the system, presenting a robust behaviour. The results obtained for the proposed scheme are satisfactory since the IAE and the injection time of the pump with respect to on-off control are reduced in more than a 25%, which leads to increase the production of aminoacids, nearly 5%, because the enzymes are more time on its optimum working pH, and savings in energy and reagents. The improvements shown by the FSP + anti-windup will have great interest in the industry, with reactors of tens or hundreds of cubic meters, where the increased production and reduced production costs implies a significant increase in profits.

Acknowledgements

This research was partially funded by the grants CTQ2008-06741-CO2-01/PPQ and DPI2011-27818-C02-01, Ministry of Science and Innovation, Government of Spain.

References

Acién, F.G., Garcia, F., Sanchez, J.A., Fernández, J.M., Molina, E., 1998. Modelling of biomass productivity in tubular photobioreactors for microalgal cultures. Effects of dilution rate, tube diameter and solar irradiance. Biotechnology and Bioengineering 58 (6), 605-616.

Acién, F.G., García, F., Sánchez, J.A., Fernández, J.M., Molina, E., 2000. Modeling of eicosapentaenoic acid (EPA) production from *Phaeodactylum tricornutum* cultures in tubular photobioreactors. Effects of dilution rate, tube diameter, and solar irradiance. Biotechnology and Bioengineering 68, 173-183.

Ayala, C.O., Roca, L., Guzmán, J.L., Normey-Rico, J.E., Berenguel, M., Yebra, L., 2011. Local model predictive controller in a solar desalination plant collector field. Renewable Energy 36, 3001-3012.

Bouhenchir, H., Cabassud, M., Le Lann, M.V., 2006. Predictive functional control for the temperature control of a chemical batch reactor. Computers and Chemical Engineering 30 (6-7), 1141-1154.

Carrasco, J., Baños, A., Arenas, A., 2009. Reset control of an industrial in-line pH process. Proc. IEEE Int. Conf. Emerg. Technol. Factory Autom. 1–8.

Cohen, G.H., Coon, G.A., 1953. Theoretical Considerations of retarded Control. ASME Transactions (EUA) 75, 827– 834.

Flesch, R.C.C., Torrico, B.C., Normey-Rico, J.E., Cavalcante, M.U., 2011. Unified approach for minimal output dead time compensation in MIMO processes. Journal of Process Control 21, 1080–1091.

Gaberalla, M., Elarafi, M.K., Hisham, S.B., 2008. Modeling and Control of pH Neutralization Using Neural Network. International Conference on Control, Automation and Systems COEX, Seoul, Korea.

González, C.V., Cerón, M.C., Acién, F.G., Bustos, C.S., Chisti, Y., Fernández, J.M., 2010. Protein measurements of microalgal and cyanobacterial biomass. Bioresource Technology 101, 7587-7591.

Guadix, A., Guadix, E.M., Páez-Dueñas, M.P., González-Tello, P., Camacho, F., 2000. Technological processes and methods of control in the hydrolysis of proteins. Ars Pharmaceutica 41 (1), 79-89.

Hua, X., Rohani, S., Jutan, A., 2004. Cascade closed-loop optimization and control of batch reactors. Chemical Engineering Science 59 (24), 5695-5708.

Jie, M., Raza, W., Xu, Y.C., Shen, Q., 2008. Preparation and optimization of amino acid chelated micronutrient fertilizer by hydrolyzation of chicken waste feathers and the effects on growth of rice. J. Plant Nutr. 31, 571-582.

Kechaou, E.S., Dumay, J., Donnay-Moreno, C., Jaouen, P., Gouygou, J.P., Bergé, J.P., Ben Amar, R., 2009. Enzymatic hydrolysis of cuttlefish (*Sepia officinalis*) and sardine (*Sardinapilchardus*)

viscera using commercial proteases: Effects on lipid distribution and amino acid composition. Journal of Bioscience and Bioengineering 107 (2), 158–164.

Kubo, M., Okajima, J., Hasumi, F., 1994. Isolation and characterization of soybean waste-degrading microorganisms and analysis of fertilizer effects of the degraded products. Appl. Environ. Microbiol. 60, 243-247.

Macků, L., Sámek, D., 2010. Two step, PID and model predictive control using artificial neural network applied on semi-batch reactor. WSEAS Transactions on Systems 9 (10), 1039-1049**.**

Margot, A., Flaschel, E., Renken, A., 1997. Empirical kinetic models for tryptic whey protein hydrolysis. Process Biochemistry 32 (3), 217-223.

Martínez, J., Camacho, O., 2005. Two new Smith predictor proposals for performance and robustness enhancement for systems with elevated time delay. Revista Técnica de la Facultad de Ingeniería Universidad del Zulia 28 (3), 11-24.

Mitchell, C.C., Hiltbold, A.E., Hue, N.V., 1994. Evaluation of a liquid potassium bicarbonate/amino acid co-product as a source of potassium, nitrogen, and sulphur. J. Plant. Nutr. 17, 2119-2134.

Morris, H.J., 2008. Cuba: Protein hydrolysates derived from green microalgae. Industrial Bioprocessing 30, 7-14.

Morris, H.J., Almarales, A., Carrillo, O., Bermúdez, R.C., 2008. Utilisation of *Chlorella vulgaris* cell biomass for the production of enzymatic protein hydrolysates. Bioresource Technol. 99 (16), 7723-7729.

Nielsen, P.M., Petersen, D., Dambmann, C., 2001. Improved method for determining food protein degree of hydrolysis. J. Food Sci. 66, 642-646.

Normey-Rico, J.E., Camacho, E.F., 1999. Robustness effects of a prefilter in a Smith predictor based. IEE Proc.-Control Theory Appl. 146 (2), 179-185.

Normey-Rico, J.E., Camacho, E.F., 2007. Control of Dead-time Processes. Springer-Verlag London Limited 2007.

Normey-Rico, J.E., Camacho, E.F., 2009. Unified approach for robust dead-time compensator design. Journal of Process Control 19, 38–47.

Ördög, V., Stirk, W.A., Lenobel, R., Bancířová, M., Strnad, M., Van Staden, J., Szigeti, J., Németh, L., 2004. Screening microalgae for some potentially useful agricultural and pharmaceutical secondary metabolites. J. Appl. Phycol. 16, 309-314.

Ordóñez, C., Asenjo, M.G., Benitez, C., González, J.L., 2001. Obtaining a protein concentrate from integral defatted sunflower flour. Bioresource Technology 78, 187-190.

Ovissipour, M., Abedian, A, Motamedzadegan, A., Rasco, B., Safari, R., Shahiri, H., 2009. The effect of enzymatic hydrolysis time and temperature on the properties of protein hydrolysates from Persian sturgeon (*Acipenserpersicus*) viscera. Food Chemistry 115, 238-242.

Palancar, M.C., Aragón, J.M., Miguéns, J.A., Torrecilla, J.S., 1996. Application of a model reference adaptive control system to pH control. Effects of lag and delay time. Industrial and Engineering Chemistry Research 35, 4100-4110.

Rebolloso, M.M., Acién, F.G., Sánchez, J.A., Guil, J.L., 2000. Biomass nutrient profiles of the microalga *Porphyridium cruentum*. Food Chemistry 70, 345-353.

Rebolloso, M.M., Navarro, A., García, F., Ramos, J.J., Guil, J.L., 2001. Biomass nutrient profiles of the microalga *Nannochloropsis*. Journal of Agricultural and Food Chemistry 49, 2966-2972.

Roca, L., Guzmán, J.L., Normey-Rico, J.E., Berenguel, M., Yebra, L., 2009. Robust constrained predictive feedback linearization controller in a solar desalination plant collector field. Control Engineering Practice 17, 1076–1088.

Roca, L., Guzmán, J.L., Normey-Rico, J.E., Berenguel, M., Yebra, L., 2011. Filtered Smith predictor with feedback linearization and constraints handling applied to a solar collector field. Solar Energy 85, 1056–1067.

Romero-García J.M., Acién, F.G., Fernández, J.M., 2012. Development of a process for the production of L-aminoacids concentrates from microalgae by enzymatic hydrolysis. Bioresource Technology 112, 164-170.

Santos, T.L.M., Botura, P.E.A., Normey-Rico, J.E., 2010. Dealing with noise in unstable dead time process control. Journal of Process Control 20, 840–847.

Sheih, I., Wu, T., Fang, T.J., 2009. Antioxidant properties of a new antioxidative peptide from algae protein waste hydrolysate in different oxidation systems. Bioresource Technology 100, 3419-3425.

Sing, C.H., Postlethwaite, B., 1997. pH control: handling nonlinearity and dead time with fuzzy relational model-based control. IEE Proc. Control Theory Appl. 144 (3), 263-268.

Smith, O.J.M., 1957. Closed control of loops with dead-time. Chem. Eng. Progress 53, 217–219.

Soetrisno, U.S.S., Holmes, Z., 1992. Functional properties of acid and salt extracted proteins of yellow peas (*Pisumsativum* L. Miranda). J. Agric. Food Chem. 40, 975-980.

Spolaore, P., Joannis-Cassan, C., Duran, E., Isambert, A., 2006. Commercial applications of microalgae. Journal of Bioscience and Bioengineering 101, 87-96.

Tang, C., Wang, X., Yang, X., 2009. Enzymatic hydrolysis of hemp (*Cannabis sativa L.*) protein isolate by various proteases and antioxidant properties of the resulting hydrolysates. Food Chemistry 114, 1484–1490.

Tejada, M., González, J.L., 2003. Influence of foliar fertilization with amino acids and humic acids on productivity and quality of Asparagus. Biol. Agric. Hortic. 21, 277-291.

Williams, G.L., Rhinehart, R.R., Riggs, J.G., 1990. In Line Process Model Based Control of Wastewater pH Using Dual. Ind. Eng. Chem. Res. 29 (7), 1254-1259.

Wright, R.A., Kravaris, C., 1991. Nonlinear Control of pH Processes Using the Strong Acid Equivalent. Ind. Eng. Chem. Res. 30 (7), 1561-1572.

Figure captions

Fig. 1. Tubular photobioreactor (3 m^3) at Estación Experimental Fundación Cajamar (EEFC) located in Almería, Spain.

Fig. 2. Block-diagram of the process for the production of free-aminoacids concentrates from *S. almeriensis* microalgae biomass (Romero-García et al., 2012).

Fig. 3. Experimental equipment. (1) Thermostat bath, (2) electrical resistance with stirrer, (3) pulse pump, (4) bypass, (5) BSTR, (6) pH-meter, (7) temperature sensor, (8) input-output card, (9) control computer.

Fig. 4. Industrial enzymatic hydrolysis control.

Fig. 5. Reaction curve for a step change of Δu introduced at t_0 instant.

Fig. 6. Smith Predictor structure.

Fig. 7. Filtered Smith Predictor structure.

Fig. 8. Model with uncertainty in the frequency domain (Normey-Rico and Camacho, 2007).

Fig. 9. Open-loop experiment 1.

Fig. 10. Open-loop experiment 2.

Fig. 11. Open-loop experiment 3.

Fig. 12. Signal filtering and model validation for pulses 2 and 6 for a fourth experiment.

Fig. 13. $F_r(s)$ design for NaOH (1M) case.

Fig. 14. $F_r(s)$ design for H_2SO_4 (1M) case.

Fig. 15. Simulation results for the resulting control law against process uncertainties.

Fig. 16. Comparison between different types of control schemes for performance with NaOH (1M) in a plant with modeling error L=90 seconds.

Fig. 17. Comparison between different types of control schemes for performance with H_2SO_4 (1M) in a plant with modeling error L=19 seconds.

Fig. 18. Anti-windup control scheme.

Fig. 19. Comparison of the real experiments between FSP+anti-windup and On-off control for the step with NaOH (1M).

Fig. 20. Comparison of the real experiments between FSP+anti-windup and On-off control for the step with H_2SO_4 (1M).

Figure 1

Fig. 1. Tubular photobioreactor (3 m^3) at Estación Experimental Fundación Cajamar (EEFC) located in Almería, Spain.

Figure 2

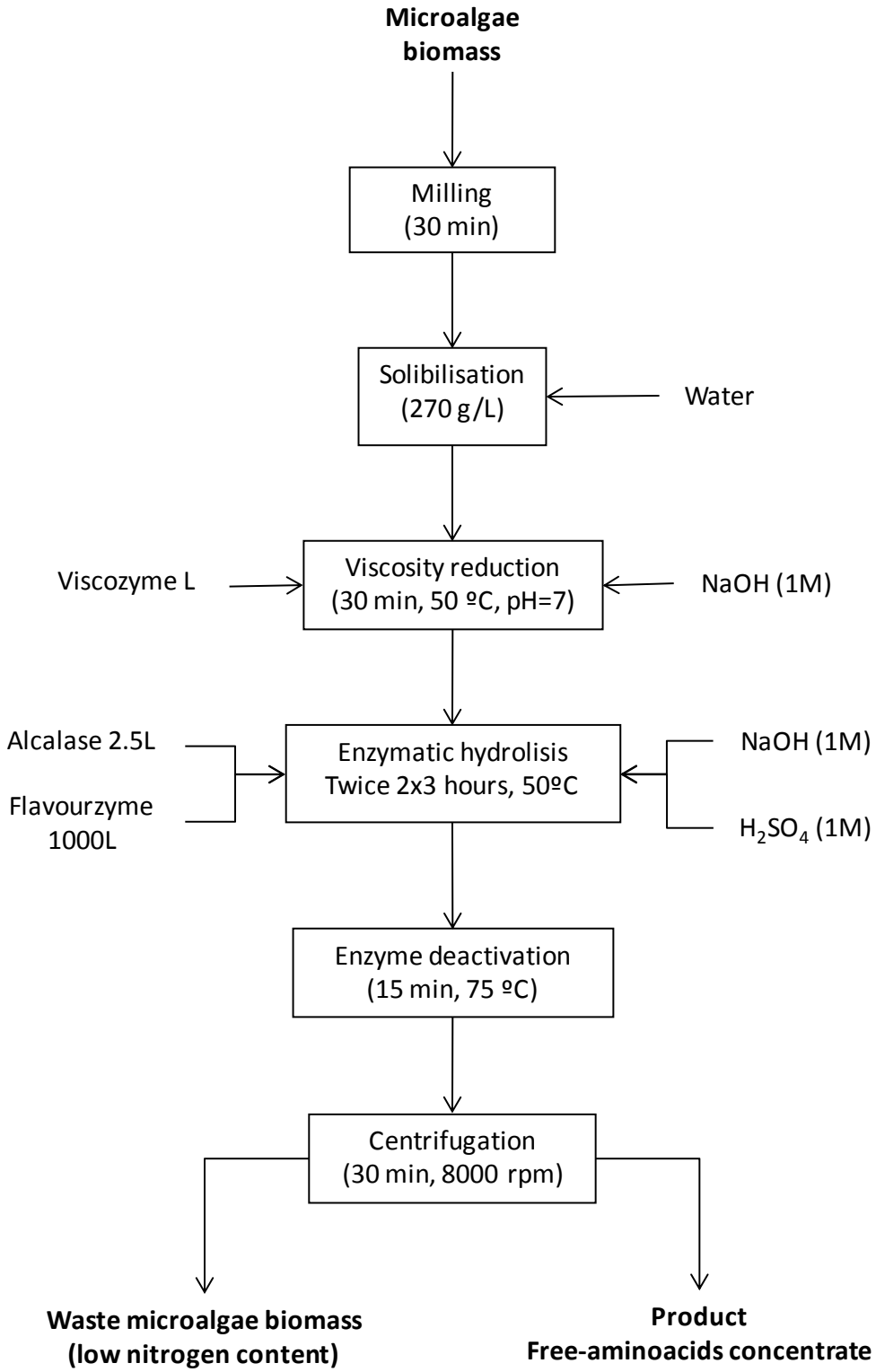

Fig. 2. Block-diagram of the process for the production of free-aminoacids concentrates from *S. almeriensis* microalgae biomass (Romero-García et al., 2012).

Figure 3

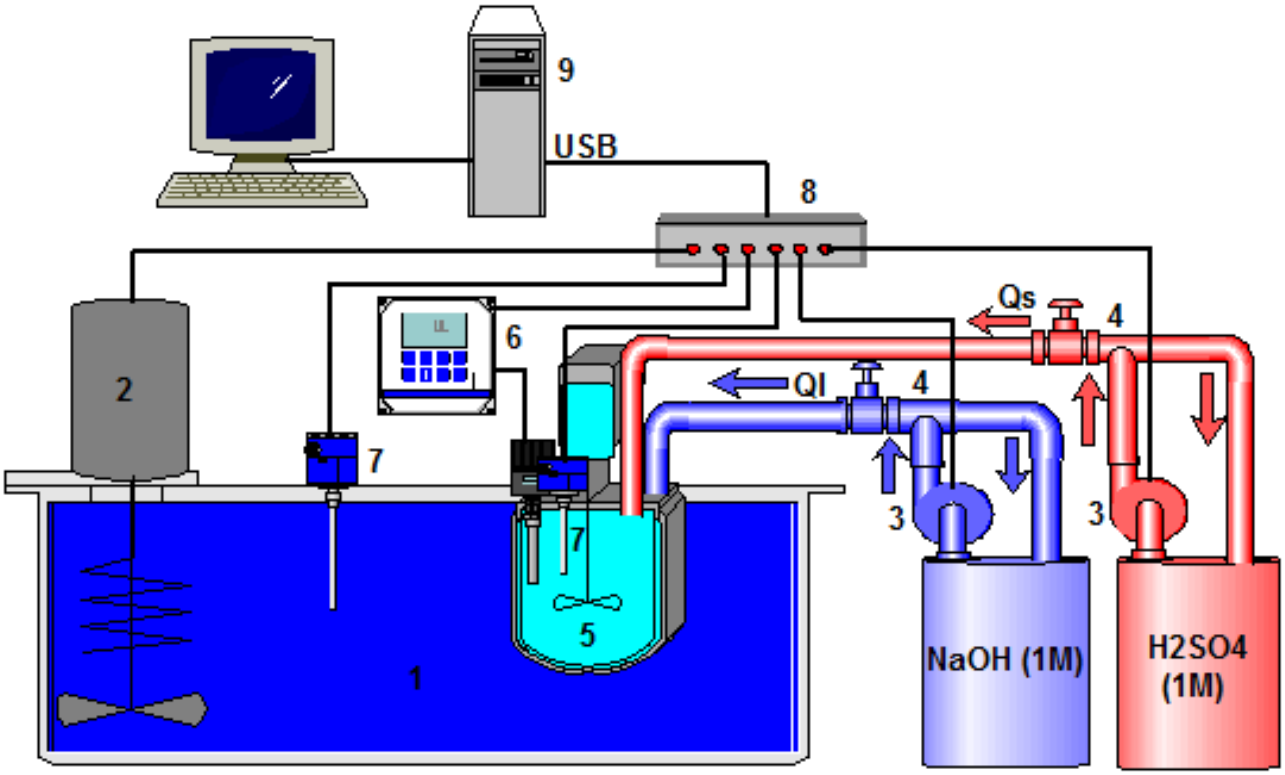

Fig. 3. Experimental equipment. (1) Thermostat bath, (2) electrical resistance with stirrer, (3) pulse pump, (4) bypass, (5) BSTR, (6) pH-meter, (7) temperature sensor, (8) input-output card, (9) control computer.

Figure 4

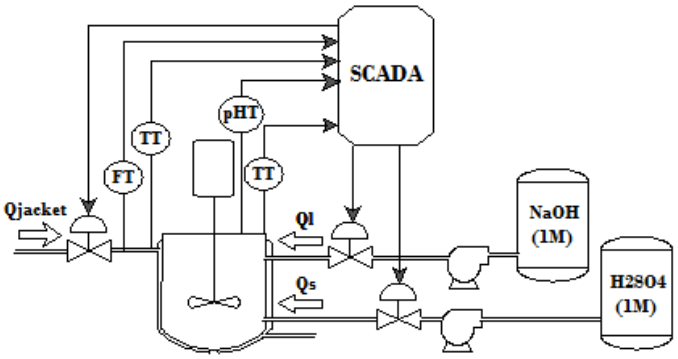

Fig. 4. Industrial enzymatic hydrolysis control.

Figure 5

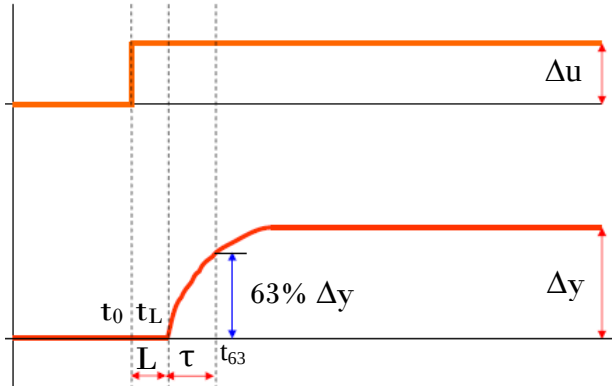

Fig. 5. Reaction curve for a step change of Δu introduced at t_0 instant.

Figure 6

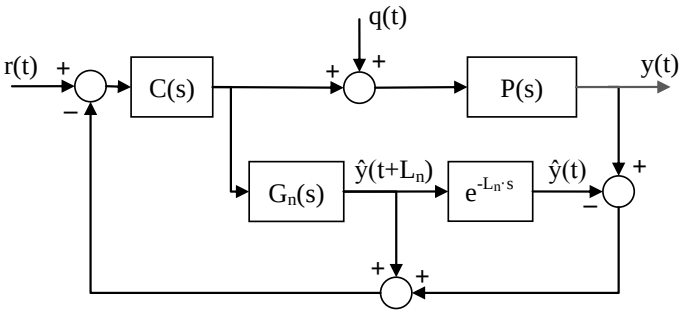

Fig. 6. Smith Predictor structure.

Figure 7

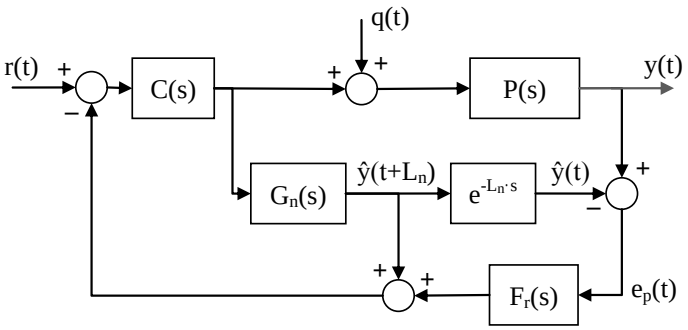

Fig. 7. Filtered Smith Predictor structure.

Figure 8

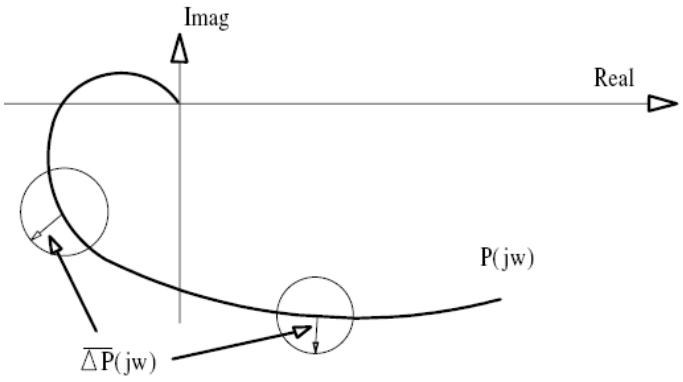

Fig. 8. Model with uncertainty in the frequency domain (Normey-Rico and Camacho, 2007).

Figure 9

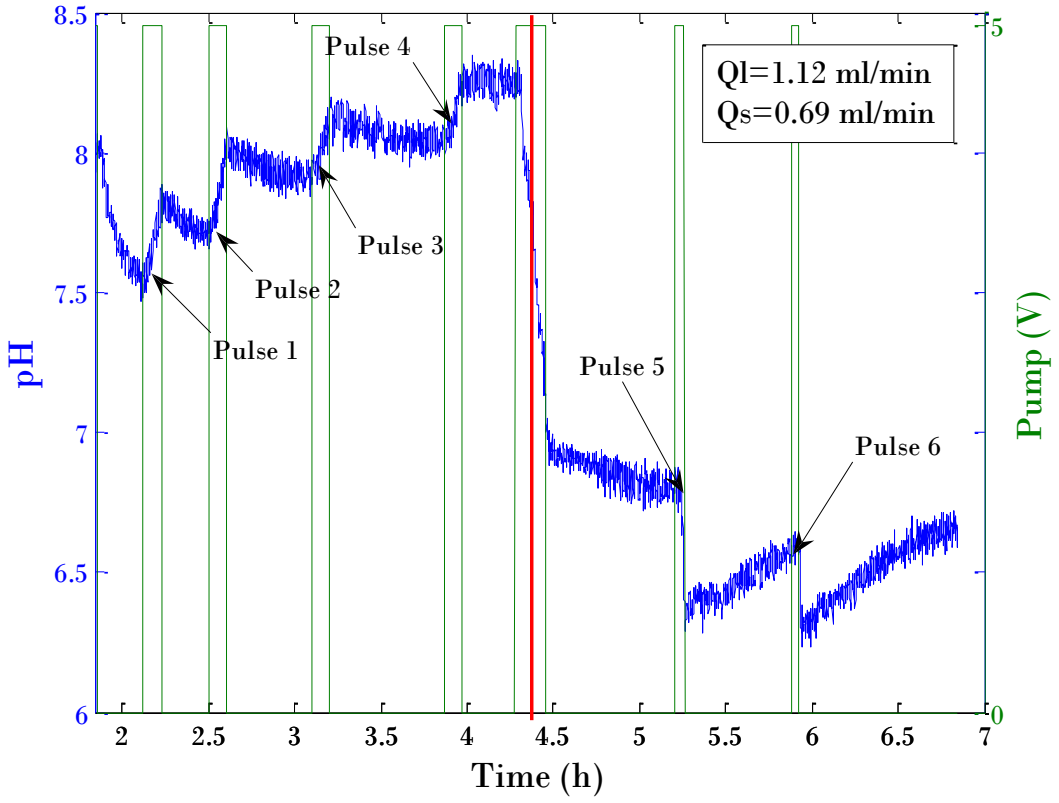

Fig. 9. Open-loop experiment 1.

Figure 10

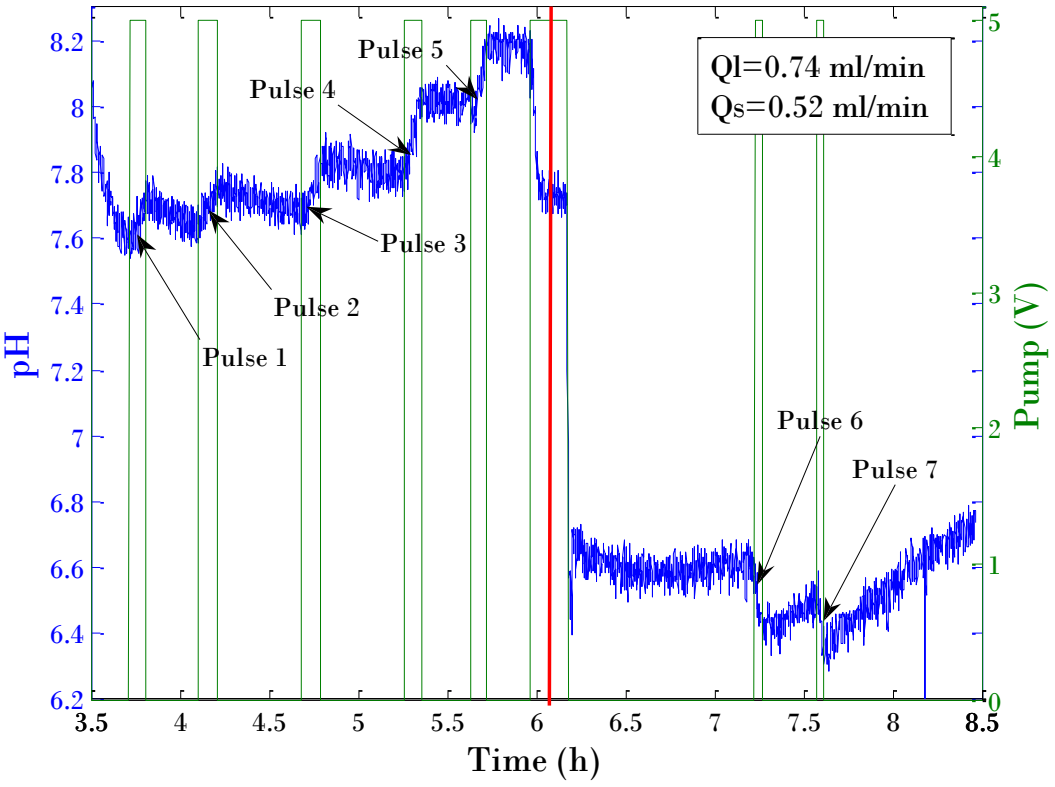

Fig. 10. Open-loop experiment 2.

Figure 11

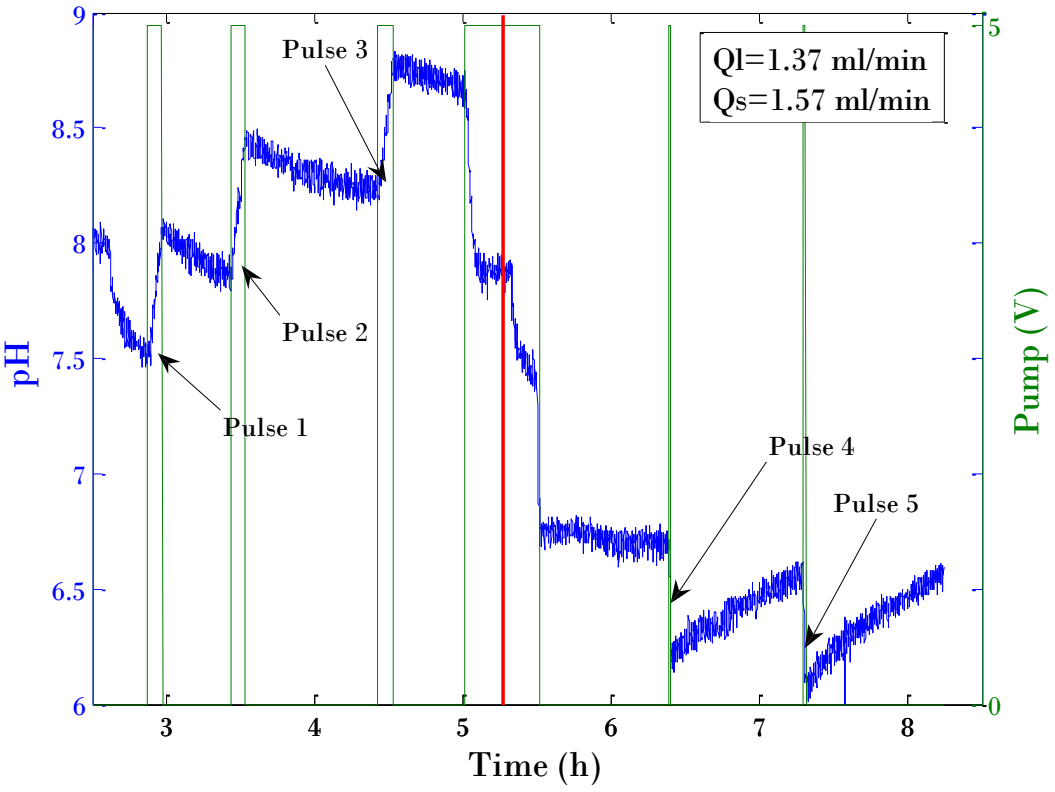

Fig. 11. Open-loop experiment 3.

Figure 12

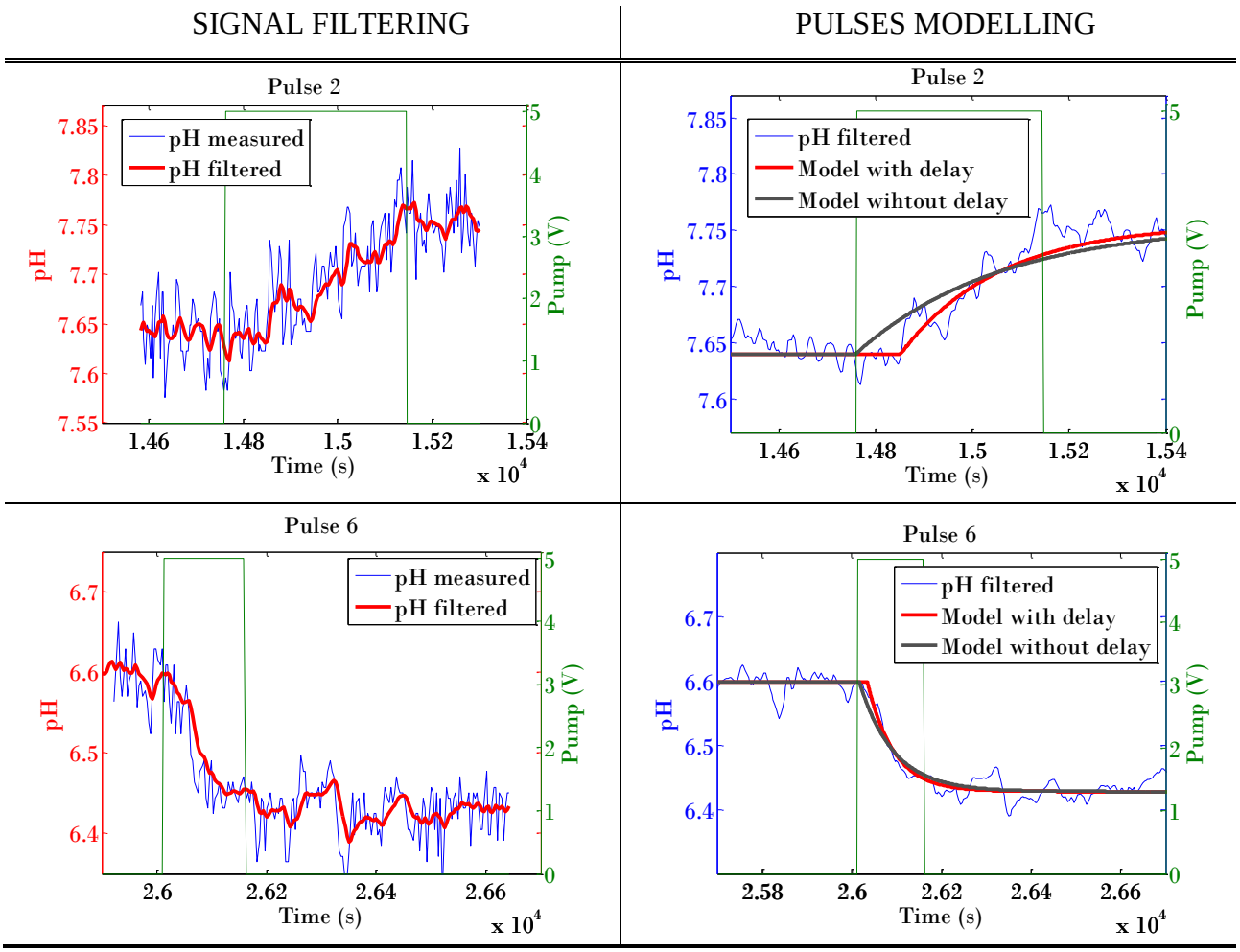

Fig. 12. Signal filtering and model validation for pulses 2 and 6 for a fourth experiment.

Figure 13

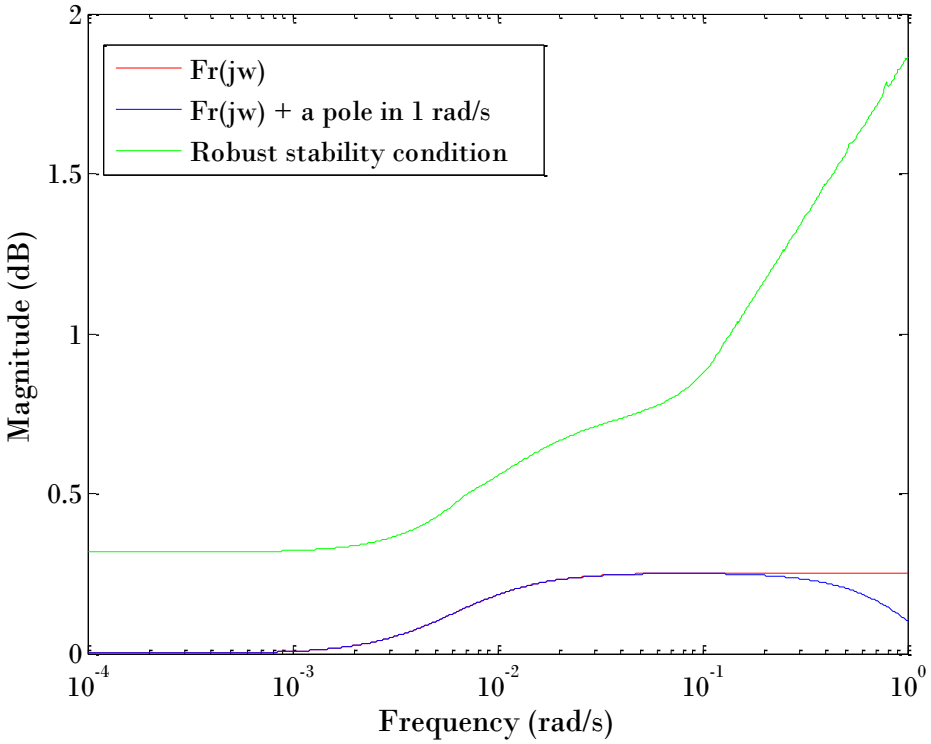

Fig. 13. $F_r(s)$ design for NaOH (1M) case.

Figure 14

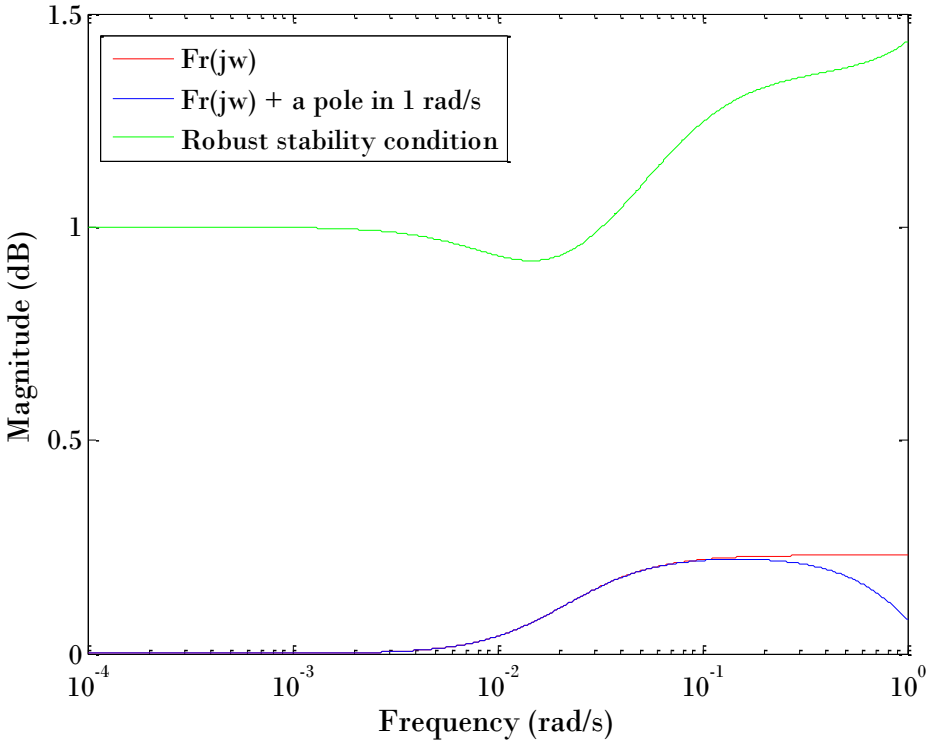

Fig. 14. *$F_r(s)$* design for H_2SO_4 (1M) case.

Figure 15

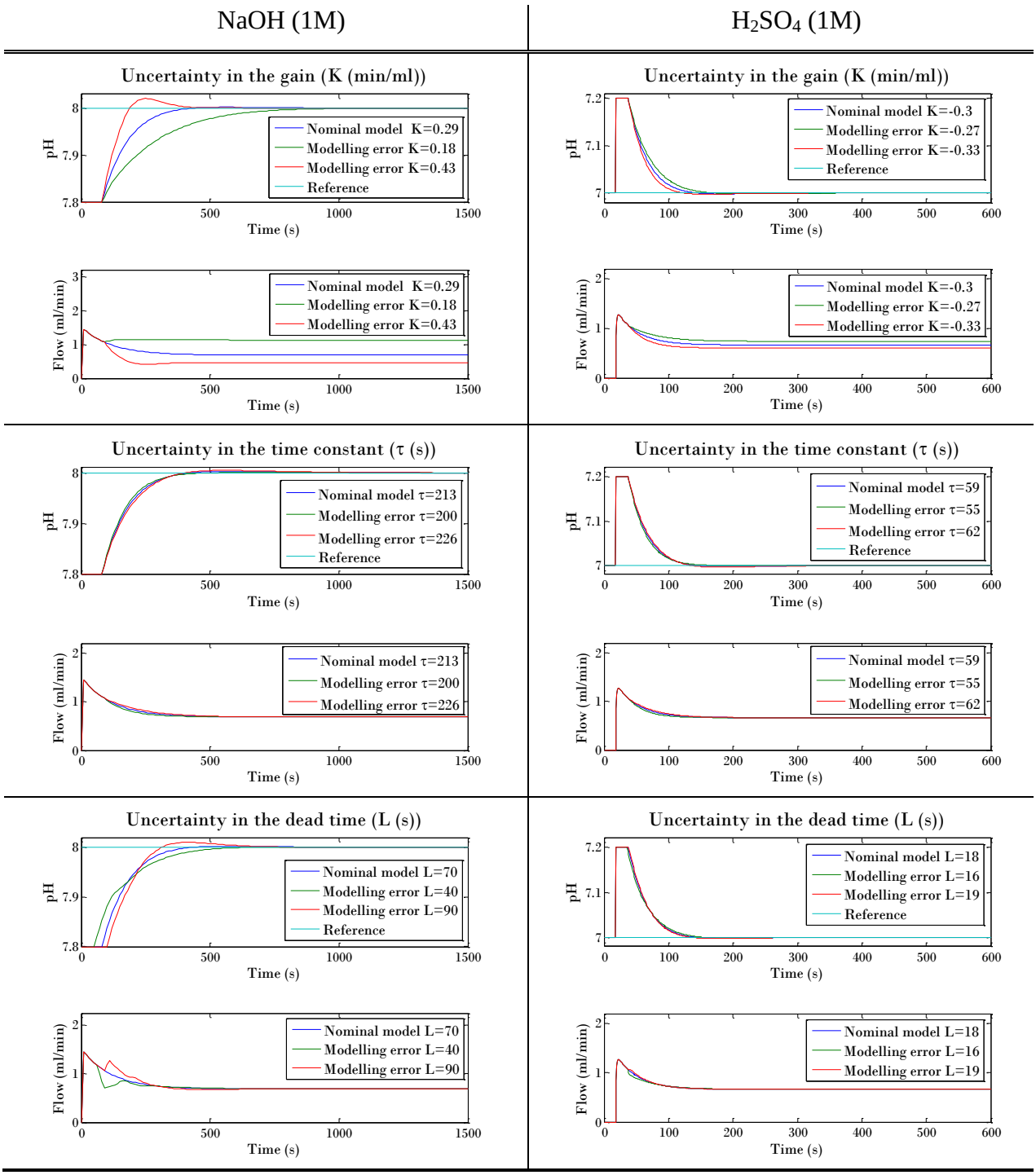

Fig. 15. Simulation results for the resulting control law against process uncertainties.

Figure 16

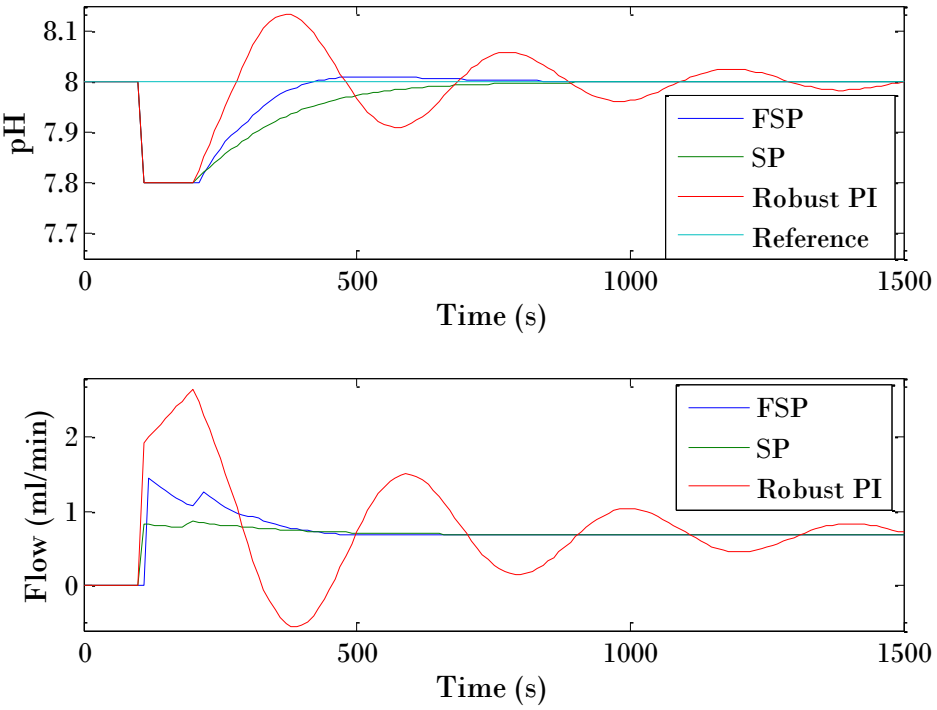

Fig. 16. Comparison between different types of control schemes for performance with NaOH (1M) in a plant with modeling error L=90 seconds.

Figure 17

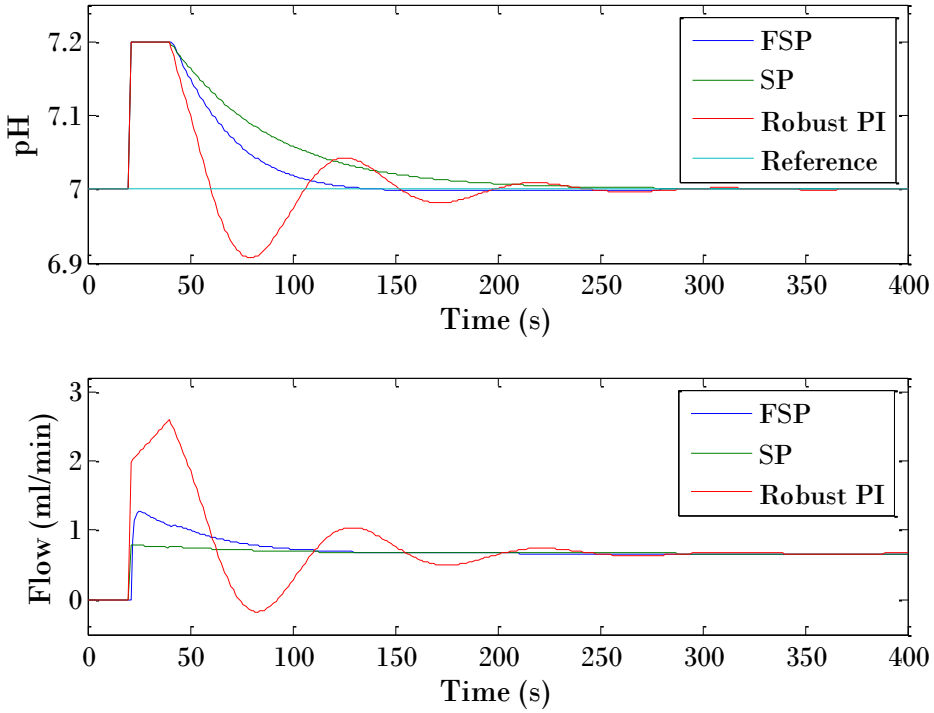

Fig. 17. Comparison between different types of control schemes for performance with H_2SO_4 (1M) in a plant with modeling error L=19 seconds.

Figure 18

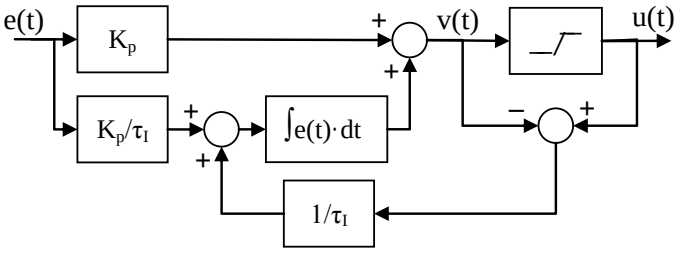

Fig. 18. Anti-windup control scheme.

Figure 19

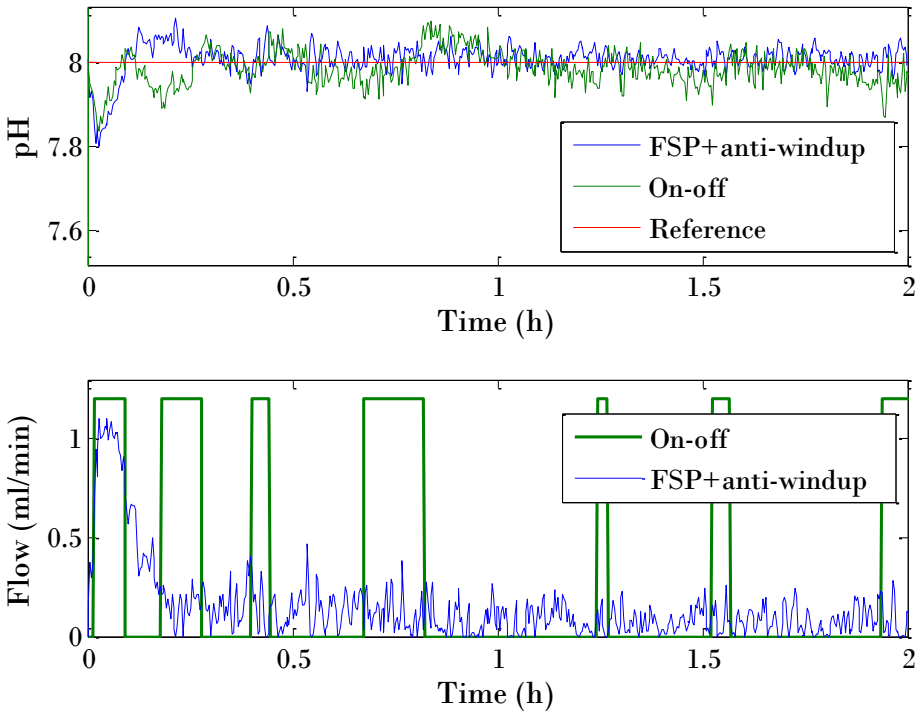

Fig. 19. Comparison of the real experiments between FSP+anti-windup and On-off control for the step with NaOH (1M).

Figure 20

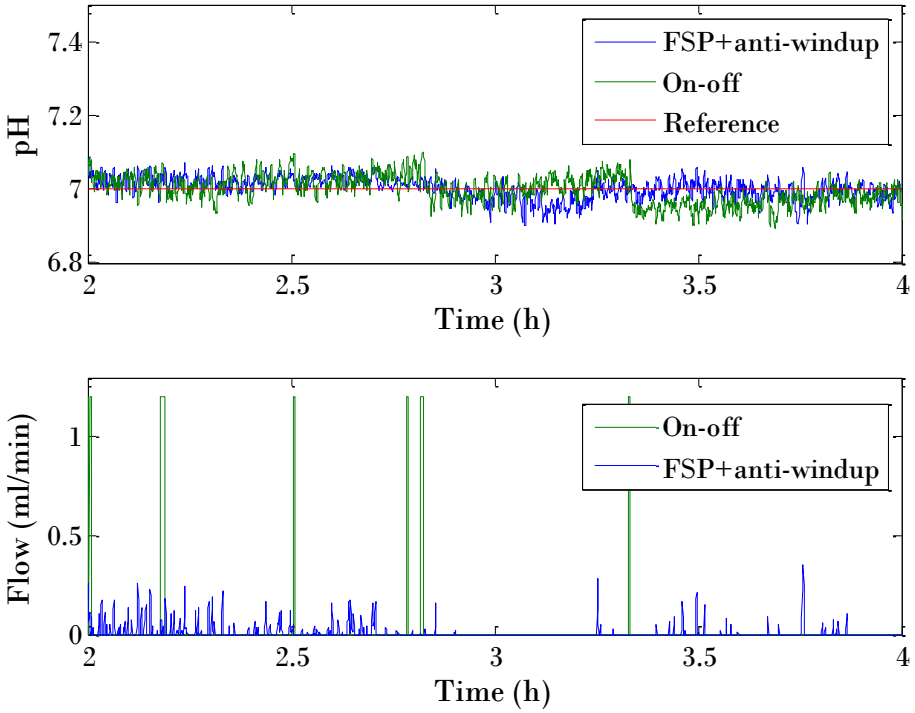

Fig. 20. Comparison of the real experiments between FSP+anti-windup and On-off control for the step with H_2SO_4 (1M).

Table 1

Model parameters.

	Model with delay			Model without delay	
Pulse	K (min/ml)	τ (s)	L (s)	K (min/ml)	τ (s)
		Experiment 1			
Pulse 1	0.25	217	53	0.25	270
Pulse 2	0.27	225	45	0.27	270
Pulse 3	0.18	226	70	0.18	296
Pulse 4	0.21	223	80	0.21	303
		Experiment 2			
Pulse 1	0.21	202	88	0.21	290
Pulse 2	0.16	206	92	0.16	298
Pulse 3	0.18	204	84	0.18	288
Pulse 4	0.32	201	57	0.32	258
Pulse 5	0.26	207	75	0.26	282
Pulse 6	-0.33	59	18	-0.33	77
Pulse 7	-0.27	62	19	-0.27	81
		Experiment 3			
Pulse 1	0.37	200	48	0.37	248
Pulse 2	0.43	205	51	0.43	256
Pulse 3	0.39	201	43	0.39	241
Pulse 4	-0.30	56	17	-0.30	73
Pulse 5	-0.33	55	16	-0.33	71

Table 2

Numerical data for real experimental results.

	NaOH (1M)		H_2SO_4 (1M)	
	FSP+ anti-windup	On-off	FSP+ anti-windup	On-off
IAE (s)	15.68	21.68	48.55	65.88
Injection time (s)	1279.54	1874.99	83.77	112.99
Hydrolysis degree (%)	46.04	43.86	7.46	7.14